Chapter 2
Optical Properties and Optical Spectroscopy of Rare Earth Ions in Solids

2.1 Electron–Phonon Coupling in Solids

The Franck-Condon principle plays an important role in understanding the nature of optical transitions in laser-active ions in solids. According to this principle, absorption of a photon is an instantaneous process during which the nuclei are enormously heavy as compared to the electrons. In other words, the electronic transition occurs on a time scale that is short compared to nuclear motion, so the transition probability can be calculated at a fixed nuclear position. An electronic transition is therefore considered to be a vertical transition. Thus, during light absorption, which occurs in femtoseconds to nanoseconds, electrons can move but nuclei cannot. The much heavier atomic nuclei have no time to readjust themselves during the absorption act; instead, they readjust after the absorption process is over, which in turn creates vibrations. This occurrence is best illustrated by potential energy diagrams. Figure 2.1 is an expanded energy-level diagram with the abscissa representing the distance between the nuclei, Q. The two potential curves show the potential energy of the optical center as a function of this distance for ground and excited states. Excitation is represented, according to the Franck-Condon principle, by a vertical (i.e., instantaneous) arrow (arrow A in Fig. 2.1). This arrow crosses the upper curve, higher than the lowest point. Appearance of the optical center after the absorption process in the excited state means that the center enters a nonequilibrium configuration and needs to relax into the lower state. This relaxation process involves radiation of phonons, which is a characteristic of the lattice vibration mode. Note that there is an exception: the case of 0–0 transition, in which the resultant absorption and emission lines are called zero-phonon lines (ZPLs). ZPLs result from transitions between the lowest vibration state of the ground electronic level and that of the excited state (not indicated in the figure).

In a Franck-Condon diagram, the relaxation process is usually denoted by a down arrow inside the individual potential curve of the electronic state (not shown in Fig. 2.1). Such relaxation processes usually take place in femtoseconds to nanoseconds. During the relaxation process, almost all of the vibration energy in

V. Ter-Mikirtychev, *Fundamentals of Fiber Lasers and Fiber Amplifiers*,
Springer Series in Optical Sciences 181, DOI: 10.1007/978-3-319-02338-0_2,

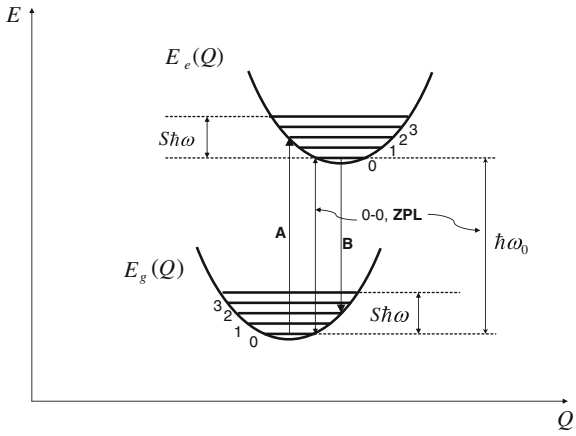

Fig. 2.1 Franck-Condon diagram of the ground and excited states of the optical center in solids. The *vertical axis* represents energy and the *horizontal axis* denotes the value proportional to the distance (i.e., normal coordinate). $E_e(Q)$ and $E_g(Q)$ are the excited and ground state energies, respectively. S is the Huang-Rhys factor (see text) and $\hbar\omega$ is an effective phonon energy of the host material (i.e., the medium in which the optical center is put). *Arrow A* denotes the absorption and *arrow B* denotes emission transitions

the excited center is lost by the energy exchange with the phonon reservoir (i.e., lattice of the host material), producing heat in the system. After the relaxation, the center needs to relax further through the electron transition between excited and ground electron levels. This process is called *luminescence*, starting from near the bottom of the upper potential curve and following a vertical arrow down (arrow *B* in Fig. 2.1), until it crosses the lower potential curve. Similar to the absorption process described previously, the luminescence transition (down arrow) does not cross the deepest point of the ground state (again, except for the previously mentioned 0–0 transition), and some excitation energy gets converted to the vibration energy. As shown in the diagram, the absorption-emission process contains two periods of energy dissipation; this phenomenon in turn creates a Stokes shift—a process during which the emission spectrum has a luminescence frequency lower than the related absorption frequency. (This phenomenon is also called a "red shift" because wavelengths of the emission are longer than of the absorption). Note that in the case of a nonlinear absorption process, such as up-conversion (i.e., the process in which two or more pump photons are used to get an ion to its high exciting level with subsequent emission of photons with higher than the original energy), the wavelength of luminescence is shorter than that of absorption. Such phenomena are widely used for the development of short-wavelength lasers for the visible spectral range (up-conversion lasers), but they are beyond the scope of this book.

2.2 Phonon Sidebands of Optical Transition in Solids

During electronic transitions in solids, an optical center (usually an imperfection in the lattice of the crystal or glass structure) may demonstrate a change in its center-to-lattice bonding configuration in the vicinity of the optical center, which in turn affects the vibration characteristics of the host material. These modified vibration characteristics of the host solid material contribute to the nature of the pure electronic transition and create a vibronic transition of the center. Therefore, most optical defects in solids, especially those that do not have a screening electronic shell (e.g., color centers, some ions of transition metals), demonstrate not only purely electronic transitions but also a vibronic transition or what is known as a "phonon sideband." Note, however, that the strength of this center-to-lattice bonding affects the visibility of the purely electronic transition, which sometimes is visible only at cryogenic temperatures; for example, F-centers have a very strong electron–phonon coupling (which will be discussed in detail later). In contrast to this, in trivalent rare earth ions, the laser-active electronic transitions are screened from the lattice environment by an electronic shell of the ion. In these optical systems, a well-resolved and intense electronic transition is evident already at room temperature with very weak electron–phonon couplings (i.e., phonon sideband). Therefore, trivalent rare earth ions, such as Er^{3+}, Yb^{3+}, and Nd^{3+}, are examples of optical systems with weak electron–phonon couplings.

To quantitatively characterize an electron–phonon coupling and its strength, let us again consider the Franck-Condon diagram shown in Fig. 2.1. In this figure, the excited and ground states have energies $E_e(Q)$ and $E_g(Q)$, respectively, with separation between the lowest vibration states of the upper and lower levels of $E_0 = hv_0$. Absorption and emission spectra commonly comprise of a number of peaks (which are usually resolved very well at cryogenic temperatures) corresponding to the number of phonons involved in the transition and thus reflecting a vibronic structure of the final electronic level (i.e., where the transition is terminated). The probability of such a multiphonon transition can be expressed as follows:

$$P_n = \frac{S^n}{n!}\exp(-S) \tag{2.1}$$

where n is number of phonons involved in the transition and S is the Huang-Rhys factor, the physical meaning of which is in the strength of the electron–phonon coupling. This expression in turn reflects the schematic shape of the phonon sideband of the optical transition. In the spectrum of optical transition, the phonon sideband is a spectral band adjacent to the line of the pure electronic transition.

The most probable transition (emission or absorption) takes place with emission or absorption of the energy equal to the following:

$$E_{\substack{\text{em}\\\text{abs}}} = hv_0 \mp Shv \tag{2.2}$$

where S (the same Huang-Rhys factor) indicates the number of phonons involved in the corresponding transition process, h is the Planck constant and v is the frequency.

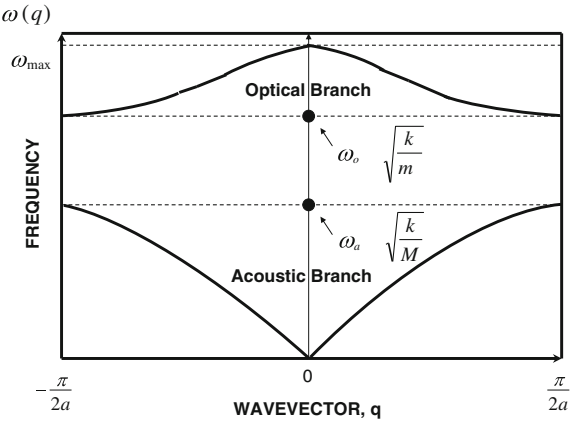

Fig. 2.2 One-dimensional phonon dispersion *curves* for a linear diatomic chain structure. The *top line* corresponds to the optical branch and the *lower curve* corresponds to the acoustic branch. See text for details

It is also useful to mention two types of lattice vibration modes in solids that have a direct relationship with some nonlinear scattering processes. In the case of a one-dimensional chain of atoms with a unit cell of two atoms, a phonon dispersion shows only one acoustic and one optical branch:

$$\omega^2(q) = \frac{k}{m^*} \pm k\sqrt{\frac{1}{(m^*)^2} - \frac{4\sin^2(qa)}{mM}} \tag{2.3}$$

where q is a wave vector, k is the force constant (i.e., elastic constant, measured in units $\left[\frac{H}{m} = \frac{\text{kg}}{\text{sec}^2}\right]$), a is the interatomic distance, m and M are the atomic masses, and $1/m^* = 1/m + 1/M$, where m^* is the effective mass. The acoustic and optic branches are specified by "±", with minus (−) for acoustical and plus (+) for optical. The two phonon branches can be seen in Fig. 2.2. The higher energy branch is optical and the lower energy branch is acoustical.

Later in the book, nonlinear scattering processes that take place in fibers will be discussed. These processes play an important role in the power scaling of fiber lasers. Each of the phonon branches described previously participates in different stimulated scattering processes, namely optical (stimulated Raman scattering) and acoustical (stimulated Brillouin scattering).

2.3 Optical Center Transitions: Spontaneous and Stimulated Emission

Consider an atomic system with discrete energy levels, which are annotated here as 1 and 2. The corresponding energy states of the levels are E_1 and E_2. E_2 is assigned a higher level, as follows:

$$E_1 < E_2 \tag{2.4}$$

In the case of thermal equilibrium, the population density of each energy level follows the Boltzmann statistics, according to which

$$N_2 = N_1 \exp\left(-\frac{E_2 - E_1}{k_B T}\right) \tag{2.5}$$

where k_B is the Boltzmann constant and T is the absolute temperature of the system. It is evident from Eq. 2.5 that the density population of the higher energy level E_2 is less than that of the lower energy level E_1 in thermal equilibrium. When an atom absorbs light with photon energy equal to the energy separation between two levels, the particle goes from lower level E_1 to higher level E_2. The absorbed photon energy is as follows:

$$h\nu_a = E_2 - E_1 \tag{2.6}$$

where h is the Planck constant and ν_a is the frequency of the absorbed light quantum. Once the atom appears in excited state E_2 (which is the nonequilibrium state of the atom), the atom has a few options to relax back into its original, equilibrium state E_1. In the absence of any existing external photons, the first way is to emit the energy through a so-called spontaneous decay, which can be done by either emitting a light quantum or nonradiatively by exchanging energy with the host material (which is usually done by emitting phonons that are vibration modes of the host material). The light-emitting part of the spontaneous decay into the lower energy level (i.e., spontaneous light emission) is represented by the A_{21} coefficient, which is called the Einstein coefficient after Albert Einstein, who studied these processes in the early 20th century. The physical meaning of the Einstein coefficient A_{21} is the probability at which the atom decays spontaneously from E_2 to E_1 and is obviously related to lifetime of the excited state of the atom.

However, if there is an external light photon with energy close to the separation $E_2 - E_1$ while the atomic system is in the excited state E_2, the excited atoms can decay to the lower energy level E_1 through so-called stimulated emission. This channel of this atomic decay was introduced by Einstein. The distinctive features of the stimulated emission is that the emission produces photons that have the same energy (or frequency) as the original external photon and also have the same phase. In other words, the incident photon stimulates an emission by forcing (or inducing) the atom to relax into its lower state by producing a stimulated emission of photons at the original (i.e., incident to the atom) photon energy and its original phase.

Because of the external inducing force, the stimulated processes can drive the atom not only from the higher energy state to the lower but also from the lower energy state to the higher (i.e., through stimulated emission and absorption). The probability of each of these processes (i.e., W_{21} or W_{12}) is proportional to the density of the incident electromagnetic radiation energy in the unit of spectral interval $\rho_\nu(\nu)$ (spectral energy density). The coefficient of proportionality for such

probabilities in this relationship is the so-called Einstein B coefficient (B_{21} and B_{12}, for emission and absorption, respectively). In the general case, $B_{21} = \frac{g_1}{g_2} \cdot B_{12}$, where g_1 and g_2 are degeneracy terms for the lower and upper energy levels. The expression for the stimulated process probabilities, which hold for non-degenerated levels, with $g_1 = g_2 = 1$, becomes the following:

$$W_{ij} = B_{ij}\rho_v(v) \tag{2.7}$$

Note that the function $\rho_v(v)$ is a radiation density per unit frequency interval that describes the number of photons with frequencies between v and $v + \Delta v$. The total energy density ρ therefore can be obtained by integrating the spectral distribution over the whole spectral range.

Another function that has to be introduced here is the spectral line profile shape $g(v)$, which is normalized over the whole spectral range of consideration as follows:

$$\int g(v)\mathrm{d}v = 1 \tag{2.8}$$

Consider the rate of the atomic energy level population exchange in units of number of atoms per unit volume per unit time. The number of atoms leaving the level will be negative and the number of atoms entering the level will be positive.

Using notations for all three processes in the case of the nondegenerated levels ($g_1 = g_2 = 1$) introduced previously, Eq. 2.9 gives a balance of emission and absorption processes for level E_2:

$$\frac{\mathrm{d}N_2}{\mathrm{d}t} = N_1 B_{12}\rho_v(v_0) - N_2 B_{21}\rho_v(v_0) - N_2 A_{21} \tag{2.9}$$

In the case of thermal equilibrium when $\mathrm{d}N_2/\mathrm{d}t = 0$, using an expression for population densities in equilibrium within Boltzmann statistics results in the following:

$$\exp(-hv_0/(k_B T)) = \frac{B_{12}\rho_v(v_0)}{B_{21}\rho_v(v_0) + A_{21}} \tag{2.10}$$

Therefore, resolving Eq. 2.10 for $\rho_v(v_0)$ gives the following expression for the energy spectral density for blackbody radiation:

$$\rho_v(v_0) = \frac{A_{21}}{B_{21}} \frac{1}{\left(\frac{B_{12}}{B_{21}}\right)\exp\left(hv_0/(k_B T)\right) - 1} \tag{2.11}$$

Again, it must be stressed that Eq. 2.11 for blackbody radiation spectral density is for the case of thermal equilibrium.

Equation 2.12 was derived by Planck for blackbody radiation for the case of absence of nonradiative processes:

$$\rho_v(v_0) = \frac{8\pi h v^3}{\left(\frac{c}{n}\right)^3} \frac{1}{\exp\left(h v_0 / k_B T\right) - 1} \tag{2.12}$$

where c is the speed of light and n is the refractive index of the medium.

Using the Planck and Einstein relationships, the following expressions are ready for Einstein coefficients:

$$B_{21} = B_{12} \tag{2.13}$$

and

$$A_{21} = \frac{8\pi h n^3 v^3}{c^3} B_{21} \tag{2.14}$$

Equations 2.13 and 2.14 are very important for laser physics because they relate fundamental parameters of the laser material, such as spontaneous and stimulated emission probabilities, which in turn determine the laser gain.

2.4 Rare Earth Centers in Solids

This section reviews the basic properties of the most interesting rare earth ions for fiber lasers. The physics of rare earth ions is very interesting. However, in solid-state laser materials such as doped crystals and glasses, the most interesting rare earth ions are those in the lanthanum group—that is, the lanthanides. These ions usually appear in a trivalent state. The 4f electron shell determines the optical properties of lanthanides; it is almost insensitive to the surrounding atom of the host environment because of screening by 5s and 5p electron shells. This is the reason for weak interaction between optical centers and the crystalline field (weak electron–phonon coupling). Such weak interactions between the 4f electrons and the crystalline field produce a very well-resolved Stark structure of the levels, which varies slightly (compared with 3d ions, for example) from host to host. For the same reason, electronic transitions in trivalent rare earth ions are very narrow and demonstrate very weak phonon bands.

The spectral shape of the optical transitions of lanthanides in glasses is determined mostly by the following factors:

1. Stark splitting of the degenerated energy levels of the free ion, determining the number of Stark levels.
2. Magnitude of the splitting, which is determined by the host material.
3. Different line broadening mechanisms, such as homogeneous and inhomogeneous broadening.

Optical transitions between individual Stark levels contribute to the total absorption and emission line shape. Typical spectral line width of the lanthanide in

glass is approximately a few hundred wave-numbers. As an example of host material influence, oxide glasses demonstrate larger spectral line widths for lanthanides compared with that of fluoride glasses.

2.5 Homogeneous and Inhomogeneous Line Broadening

The nature of spectral line broadening plays a very important role in the performance of the solid-state laser. In particular, pump conversion efficiencies of certain laser regimes, such as single-frequency operation, heavily depend on the type of broadening of the laser line. This section reviews the basic properties of optical transition line broadening. The determination of whether the transition line shape is homogeneously or inhomogeneously broadened is based on whether the lines are from the same type of centers or from different types. In the case of rare earth ions in glasses, homogeneous and inhomogeneous broadening are the two main mechanisms of optical transition line broadening. These two mechanisms contribute almost equally to the resultant spectral line width, with an individual contribution of up to several hundred wave-numbers at 300 K. The spectral line broadening at room temperature smooths the overall line shape, which becomes resolved only at low temperatures. With a temperature decrease, Stark level structure becomes more and more evident and determines the line shape characteristic profile.

2.5.1 Homogeneous Broadening

Purely radiative decay (i.e., spontaneous decay) is described by an exponential function; the corresponding spectral line has the shape of a delta function. A good example of such radiative transition is a low-temperature zero-phonon line that occurs between the lowest vibration level of the excited state and the lowest vibration level of the lower electronic level. In the case of rare earth ions (especially in crystals), such zero-phonon transitions occur between electronic states of the Stark systems of energy levels because the strength of an electron–phonon interaction in this case is low.

Usually, a homogeneous broadening of optical centers in solids is defined by the random perturbation of the optical centers, such as the interaction with lattice phonons or an interaction with optical centers of a similar type. Such types of interactions result in shortening of the excited state lifetime of the optical center. The optical transition line shape in the case of homogeneous broadening is described by a Lorentzian function g_L (see Fig. 2.3), which is expressed as follows:

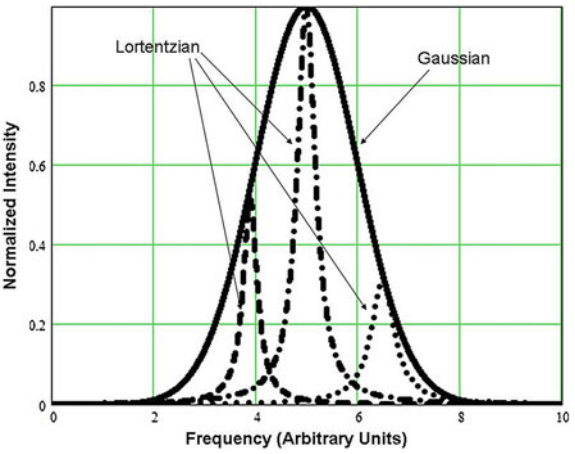

Fig. 2.3 Inhomogeneously broadened emission line spectral profile (*Gaussian shape*) and homogeneously broadened lines inside the Gaussian envelope (*Lorentzian shape*)

$$g_L(v) = \frac{\Delta v_H/(2\pi)}{(v - v_0)^2 - \left(\frac{\Delta v_H}{2}\right)^2} \tag{2.15}$$

where v_0 is the central frequency of the optical transition and Δv_H is the transition spectral line full width at half maximum (FWHM). Equation 2.15 for the Lorentzian function g_L is normalized by $\int_{-\infty}^{+\infty} g_L(v)\mathrm{d}v$.

The optical center lifetime is determined by the probability of transition from the upper level to the lower level of the optical center. This probability in turn is a sum of several process probabilities related to radiative and nonradiative transitions in the optical center. A general analytical expression for the optical center lifetime τ can be written as follows:

$$\frac{1}{\tau} = W_R + W_{\mathrm{NR}} \tag{2.16}$$

where W_R is the probability of radiative transition, which is equal to the Einstein A coefficient $A_{21} = \frac{1}{\tau_R}$. W_{NR} is the probability of all nonradiative processes of the optical center when it relaxes from the upper energy level to the lower energy level; it includes the probability of the ion interaction with phonons of the lattice, probability of ion–ion interaction, etc. In many cases, measurement of the luminescence decay time at low temperatures, such as liquid nitrogen temperatures (~77 K) or close to helium temperatures (<10 K), produces longer measured decay time by eliminating phonon interaction and therefore giving a value of purely radiative lifetime τ_R. Knowing radiative lifetime and decay time at given elevated temperature, one can determine a luminescence quantum yield—a parameter that shows a fraction of overall probability of the center transition from the higher to lower energy level, which is radiative. The luminescence quantum yield is determined by the following expression:

$$\eta_{\mathrm{LQE}} = \frac{W_R}{W_R + W_{\mathrm{NR}}} \tag{2.17}$$

Typical values of the room temperature luminescence decay in rare earth ions in solids (which is a result of the radiative and nonradiative transitions occurring in these optical centers) span from microseconds to milliseconds and are dependent on the particular ion and the host material. For example, in glass at room temperature, the lifetime of Yb^{3+} and Er^{3+} ions in their most important laser transitions are typically 1 and 10 ms, respectively.

Because of the higher phonon energy in silica glass than in phosphate glass, the probability of a nonradiative transition for a given gap between higher and lower energy levels is higher in silica glass because it requires a smaller number of participating phonons to fill the gap during relaxation from the upper level; this demonstrates the influence of the host material (energy gap law will be described in detail later in the book). In turn, this fact explains why homogeneous broadening in silica glass is usually greater than in phosphate glass. At low levels of doping, the ion–ion interaction between rare earth ions is very low; nonradiative transition probabilities originate mostly from electron exchange with lattice phonons. However, with an increase of the doping level, ion–ion interaction becomes more and more significant and may result in concentration quenching of luminescence, which affects the optical center luminescence quantum yield. In turn, this sets a limit for doping concentration levels in fibers and laser hosts in general. Other factors may also affect the decision to limit concentration of the laser-active ions at a certain concentration level.

2.5.2 Inhomogeneous Broadening

Inhomogeneous broadening of the optical center's line shape during a transition between energy levels originates from a local site-to-site variation in the optical center's surrounding field in the lattice environment. The strength and symmetry of the field around the rare earth ion determine the spectral properties of the optical transitions, as well as the transition strength. In the case of inhomogeneous broadening, the overall shape of the spectral line is a superposition of all individual, homogenously broadened lines corresponding to different types of the optical center. The line shape of the inhomogeneously broadened optical transition is described by the Gaussian line profile (see Fig. 2.3), which can be expressed as the following function of frequency:

$$g_G(\nu) = \frac{1}{\Delta\nu_{\mathrm{INH}}}\sqrt{\frac{4\ln 2}{\pi}}\exp\left[-4\ln 2\left(\frac{\nu-\nu_0}{\Delta\nu_{\mathrm{INH}}}\right)^2\right] \tag{2.18}$$

Table 2.1 Homogenous and inhomogeneous line widths for several rare earth ions in different glass hosts measured at 300 K

Rare earth ion	Glass matrix	$\Delta\nu_H$ (cm^{-1})	$\Delta\nu_{INH}$ (cm^{-1})	Source
Nd^{3+}	Silicate	110	50	[1]
Yb^{3+}	Phosphate	80	66	[2]
Er^{3+}	Germano-silicate	17	30	[3–5]
Tm^{3+}	ZBLAN (ZrF_4-BaF_2-LaF_3-AlF_3-NaF)	32	450	[6]

where $\Delta\nu_{INH}$ is the FWHM of the inhomogeneously broadened line. Determined by the optical center surrounding fields, the inhomogeneous line width is insensitive to the temperature of the host material.

In a real situation at room temperature, the individual contribution to the optical transition overall line shape by homogeneous and inhomogeneous broadening may be different or even comparable, such as in the case of most rare earth ions in glasses. In this general case, the resultant overall line shape is best described by the so-called Voigt function, which is a convolution between Lorentzian and Gaussian profiles:

$$g_{VOIGT}(\nu) = \int g_G(\xi) g_L(\nu - \xi) \mathrm{d}\xi$$

Table 2.1 demonstrates several examples of homogeneous and inhomogeneous line widths for widely used rare earth ions in some glasses at room temperature.

Note that the homogeneous and inhomogeneous line width contribution varies for the same rare earth center in different glasses. For example, it has been shown that inhomogeneous broadening of the ${}^4I_{13/2} \rightarrow {}^4I_{15/2}$ in Er^{3+}-doped silica glass was greater in alumino-silicate glasses compared to germano-silicate glass [3–5].

In optical spectroscopic research, to get information regarding the inhomogeneous broadening nature of the spectral line, one needs to cool down the host material to low temperatures (usually <77 K) in order to "freeze" phonons and eliminate contributions from homogeneous broadening. In this way, one may determine several important parameters of optical centers, such as the Stark structure of the energy levels.

2.6 Spectroscopic Parameters of the Optical Transition: A Brief Introduction to the Main Theories

Determining the spectral parameters of laser-active ions in solids is a very important task in laser physics. Several theories have been developed to calculate emission and absorption cross-sections using some of the measured spectral parameters. Existing theories reflect practical situations that appear in real solids doped with laser-active ions. This section briefly reviews each of the main theories.

2.6.1 Judd-Ofelt Theory

The Judd-Ofelt theory [7, 8] allows one to predict the stimulated emission cross-section peaks and integrated values for transitions between any level of the ion. The theory is based on the assumption that the average energy difference between the 4f levels is much larger than the energy spread of the excited configuration. The radiative transition rates and the radiative lifetimes can be obtained from the oscillator strengths of the transition. The theory gives the following expression for the oscillator strength of the electric dipole transition (f^{ed}) [7]:

$$f_{ij}^{ed} = \frac{8\pi^2 mv}{3h(2J+1)} \times \frac{(n^2+2)^2}{9n} \times \sum_{\lambda=2,4,6} \Omega_\lambda \left| \left\langle f^N J \middle| \middle| U_\lambda \middle| \middle| f^N J' \right\rangle \right|^2 \tag{2.19}$$

where i is the initial state of the transition, j is the final state of the transition, v is the transition frequency, n is the refractive index of the host material, m is the electron mass, and $\langle f^N J||U_\lambda||f^N J'\rangle$ are the reduced matrix elements, tabulated in [9].

Within this theory, the strength of any transition f can be determined by a set of three parameters: Ω_i ($i = 2, 4, 6$; see Eq. 2.19 for the oscillator strength). This set of parameters completely defines and parameterizes the effect of the host on the absorption and fluorescence properties of the ion's transitions between different multiplets of the $4f^N$ configuration. These parameters are calculated by performing a least-squares fit of the measured oscillator strengths to the theoretical ones. The more transitions that are taken into account during the fitting procedure, the more accurately determined and reliable the Judd-Ofelt coefficients appear to be (although this is not the case for Yb^{3+}, where the only transition between essentially two levels is presented in the electronic structure of the ion; see below). The complete set of Judd-Ofelt coefficients allows the calculation of the strength of any integrated cross-section. Judd-Ofelt parameters are presently tabulated for practically all rare earth ions in different solid materials. Table 2.2 presents the Judd-Ofelt parameters for Er^{3+} in different glass hosts (a detailed spectroscopic analysis of this ion will be done in Chap. 5).

For glasses, the calculated Judd-Ofelt parameters are average values of the parameters for each given site of the Er^{3+} ion because there is great variation of the sites that can be occupied by the ion (compared with crystals).

The Judd-Ofelt theory gives the total oscillator strength for the transition between two multiplets. The theory estimates only the integrated electric dipole oscillator strength for the particular transition (not the individual transitions between different states of the multiplet). Determination of the individual transitions' strength or cross-sections (spectral shapes) requires determination of the spectral distribution measurements of the relative emission spectra. This theory is particularly valuable for predicting strengths of transitions for which direct measurements are difficult. Accuracy of the Judd-Ofelt analysis is about 10–15 % for

Table 2.2 Judd-Ofelt parameters for Er^{3+} in different glass hosts

Glass matrix	$\Omega_2 \times 10^{-20}$ (cm^2)	$\Omega_4 \times 10^{-20}$ (cm^2)	$\Omega_6 \times 10^{-20}$ (cm^2)	Source
Germanate	6.4	0.75	0.34	[10]
Phosphate	9.92	3.74	7.36	[10]
Fluoride	1.54	1.13	1.19	[11]
	1.47	1.51	1.69	[23]
Borate	11.36	3.66	2.24	[10]
Tellurite	7.84	1.37	1.14	[10]
Gallium tellurite	6.46	1.64	1.47	[26]
ZBLAN (ZrF_4-BaF_2-LaF_3-AlF_3-NaF)	2.3	0.9	1.7	[12]
PKBAEr	8.05	1.46	2.28	[22]
NaTFP	5.92	1.07	1.44	[23]
Lead borate	3.31	1.63	1.29	[24]
ZTE	3.14	1.19	1.43	[25]
Oxyfluoride	2.75	1.25	0.76	[26]
Silica	8.15	1.43	1.22	[28]

most rare earth ions [13, 14]. Detailed treatments of the theory for the case of rare earth ions, including its successes and limitations, are available elsewhere [12, 15].

On a practical note, for fiber laser development in which Yb^{3+} glass plays a central role, it is practically impossible to perform a calculation of the Judd-Ofelt parameters and therefore calculate cross-section values using Judd-Ofelt theory because there is only a ${}^2F_{5/2} \rightarrow {}^2F_{7/2}$ transition (i.e., essentially a two-level transition) for Yb^{3+}. Other theoretical methods (described later) are used in the case of Yb^{3+} to determine cross-section values of optical transitions.

2.6.2 McCumber Theory

In a glass environment, rare earth ions demonstrate broad emission and absorption spectra; therefore, the previously introduced Einstein relationships need to be adjusted. For this important application, the McCumber theory can be used. The McCumber theory shows that all three processes described by Einstein in his theory—absorption, stimulated emission, and spontaneous decay—their cross-sections, and the radiative lifetime of an optical center in thermal equilibrium are related to each other at every single frequency using a set of theoretical formulas. These formulas are also sometimes called a generalized Einstein relationship.

Following McCumber [16], the theory assumes that the time required to establish a thermal distribution within each manifold is short compared with the lifetime of the manifold. The main theoretical conclusion of the McCumber theory is the following formula, which relates absorption and emission cross-sections at a

given frequency (unlike the Füchtbauer-Ladenburg theory, which gives the relationship between integrated cross-sections):

$$\sigma_{21}(\nu) = \sigma_{12}(\nu)\exp\left[\frac{E_{\text{ex}} - h\nu}{kT}\right] \tag{2.20}$$

where E_{ex} is the excitation energy, which is temperature dependent and is the net free energy required to excite an ion from its lower energy level to the upper level at temperature T. At room temperature, $kT \approx 161\ \text{cm}^{-1}$. According to the McCumber analysis, the emission and absorption cross-sections are equal at a certain frequency:

$$\nu_{\text{center}} = \frac{E_{\text{ex}}}{h} \tag{2.21}$$

All one needs to know is E_{ex}. To determine this important value following McCumber, another definition of this energy parameter is introduced:

$$\frac{N_+^0}{N_-^0} = \exp\left(-\frac{E_{\text{ex}}}{kT}\right) \tag{2.22}$$

where $N_\pm^0$ is the population of the upper and lower levels in unpumped material at temperature T.

However, if one knows the positions and number of all Stark components in the lower and upper energy levels, the same concentration ratio can be determined as follows:

$$\frac{N_+^0}{N_-^0} = \frac{\exp(-E_0/kT) \times \left(1 + \sum_{i=2}^{p} \exp\left(-E_{+i}/kT\right)\right)}{1 + \sum_{j=2}^{q} \exp\left(-E_{-j}/kT\right)} \tag{2.23}$$

where q and p are the number of Stark components at the ground and excited levels, respectively; E_0 is the energy separation between the lowest energy levels of the two manifolds (zero-phonon energy); and E_{+i} and E_{-j} are the energy differences between ith and jth levels.

The system of Eqs. 2.22 and 2.23 gives a path to calculate excitation energy E_{ex}, which in turn gives an opportunity to calculate absolute values of the emission and absorption cross-sections. As an example, for the case of Er^{3+} ions, Fig. 2.4 shows a spectral profile of the calculated stimulated-emission cross-section in low-fluorine fluorophosphate glass [17].

Figure 2.4 demonstrates a good fit with experimental data obtained for the same glass sample. The McCumber theory provides not only absolute values of the cross-section but its spectral distribution as well, thus giving the complete picture of the cross-section. This theory allows one to determine emission cross-section from the measured absorption cross-section and radiative lifetime. However, the McCumber theory requires knowledge of the electronic structure of the ion.

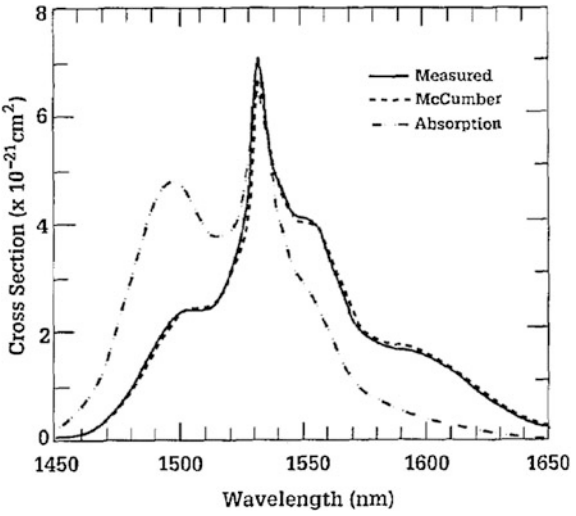

Fig. 2.4 Comparison of the shape of the measured stimulated-emission cross-section with that calculated from the absorption cross-section using the McCumber theory [17]. (Image courtesy of the optical Society of America)

Overall, the McCumber theory is a powerful instrument in hands of researchers for calculating important spectroscopic parameters of laser-active optical centers and is often used in laser physics.

2.6.3 Füchtbauer-Ladenburg Theory and Einstein Coefficients

The Füchtbauer-Ladenburg theory [18, 19] provides a relationship between the absorption coefficient and Einstein A and B coefficients for a system with two degenerate levels, using degeneracy terms g_1 and g_2 for the lower and upper energy levels. This theory assumes that in the spectral range of interest (i.e., where the optical transitions under consideration are taking place), the host material refractive index remains unchanged—an assumption that is reasonable for trivalent rare earth ions, which are being used as laser-active optical centers. The most important and probably most well-known conclusion of the Füchtbauer-Ladenburg theory is an obtained relationship between the upper-state lifetime of the laser-active ion to its emission cross-section. The corresponding Füchtbauer-Ladenburg relationship is given by:

$$\int v^2 \sigma_{21}(v) \mathrm{d}v = \frac{A_{21} c^2}{8\pi n^2} \tag{2.24}$$

where n is the refractive index; A_{21} is the Einstein coefficient, which is determined by radiative lifetime, $A_{21} = {}^1/_{\tau_{\mathrm{rad}}}$; c is the speed of light in a vacuum; v is

frequency; and $\sigma_{21}(\nu)$ is the spectral component of the emission cross-section. A similar equation can be written for the absorption cross-section:

$$\int \nu^2 \sigma_{12}(\nu) \mathrm{d}\nu = \frac{A_{21} c^2}{8\pi n^2} \frac{g_2}{g_1} \tag{2.25}$$

The relationships in Eqs. 2.24 and 2.25 give a well-known relationship between absorption and emission cross-sections:

$$g_1 \int \nu^2 \sigma_{12}(\nu) \mathrm{d}\nu = g_2 \int \nu^2 \sigma_{21}(\nu) \mathrm{d}\nu \tag{2.26}$$

A comparison of the theories presented in this chapter for calculating emission cross-sections are illustrated in Fig. 2.5 [17]. According to Fig. 2.5, the McCumber theory shows very good agreement with measured cross-section values, whereas the Einstein analysis overestimates these values.

Another example of using the Füchtbauer-Ladenburg theory for stimulated-emission cross-section calculations is illustrated in Fig. 2.6 [20]. Dong et al. [20] determined stimulated-emission cross-sections for the 3 % Nd-doped phosphate glass at both room and liquid-nitrogen temperatures using this theory.

Figure 2.6 shows variations with temperature in the stimulated-emission cross-sections of Nd:phosphate glasses calculated using the Füchtbauer-Ladenburg theory. The results show that the stimulated-emission cross-section is nearly independent of Nd^{3+} concentration. These results are important because dependence of the emission cross-section on the temperature has a significant effect on the performance of high-power Nd:glass-based lasers.

In addition to giving a path to calculate cross-sections, the Füchtbauer-Ladenburg theory shows that large emission cross-sections and therefore a

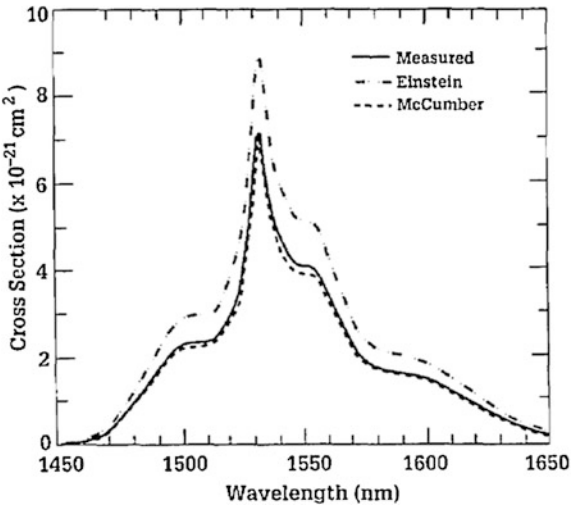

Fig. 2.5 Comparison of stimulated-emission cross-sections of Er^{3+} obtained using the radiative lifetime (measured), the Einstein relationship, and the McCumber theory with an estimated $\varepsilon \equiv E_{ex}$ for the case of fluorophosphates glass [17]. (Image courtesy of the optical Society of America.)

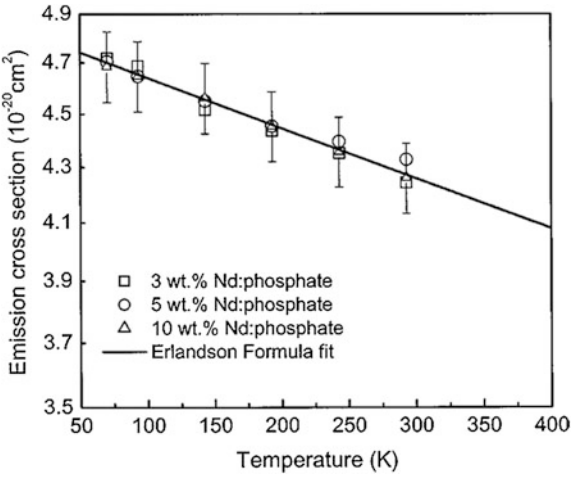

Fig. 2.6 Stimulated-emission cross-sections versus temperature for differently doped glasses. The straight line represents the model described in Ref. [20], which predicts the variation of the stimulated-emission cross-section of Nd:phosphate glasses with temperature [20, 21]. (Image courtesy of the optical Society of America.)

large-gain bandwidth of laser transitions are leading to a short radiative lifetime. This helps researchers to determine the laser-active optical centers that are required for broad-wavelength tunable laser operation and ultrashort pulse generation.

2.7 Sensitization of Laser-Active Centers

Trivalent rare earth ions used as laser-active centers in solids have several spectroscopic properties that restrict effective optical excitation for creating inversion populations. The most important spectroscopic properties that have been taken into account during rare-earth-doped gain fiber development for laser/amplifier applications are spectral line width, accessibility of the absorption band for exciting with pump-diode laser wavelengths, and absorption coefficients at the pump wavelength for reasonable gain of fiber length.

If only the most widely used laser-active rare earth centers in fiber lasers (i.e., Nd^{3+}, Yb^{3+}, Er^{3+}, and Tm) and their absorption bands are considered, we can see that all ions except for Er^{3+} require well-developed diode laser pump wavelengths of 808, 915, 976 and 792 nm when using common high-intensity excitation bands with high absorption coefficients (e.g., for Liekki Yb^{3+} [nLIGHT, Vancouver, WA], >1,200 dB/m of core absorption). Unlike the other ions mentioned, Er^{3+} demonstrates intense absorption near 1,530-nm with ~70–110 dB/m absorption coefficient and another absorption band near 980 nm with approximately one-third of that at 1,530 nm absorption band intensity. On the other hand, for high-power applications when pump-diode lasers are fiber coupled into 100–600 μm core fibers, a technology called clad pumping has been developed to make it possible to couple high-power diode lasers into the gain fibers (reviewed in detail later in this book). To use the clad pumping technique. The gain fiber consists of a doped core

and undoped cladding where the pump is coupled. However, because of the low ratio of core to clad diameter, the effective absorption of the pump light is reduced from the core absorption coefficient to the value:

$$\alpha_{\text{clad}} = \alpha_{\text{core}} \frac{S_{\text{core}}}{S_{\text{clad}}} \tag{2.27}$$

where S_{core} and S_{clad} are cross-section areas of the core and cladding, respectively. For typical true single-mode fibers with a core diameter of 9 μm and clad diameter of 125 μm, the cross-section area ratio is 0.005. Therefore, the clad pumping absorption coefficient reduces from 110 to 0.55 dB/m, which in turn requires an increase of the fiber length by a factor of 200.

One of the well-known techniques that is used to increase absorption of laser-active ions and enhance efficiency of rare-earth ion excitation is co-doping the laser active ion with another ion, using a more suitable pumping spectral location, a high doping concentration, and an efficient pumping excitation transfer to the lasing ion. Therefore, this technique is very important in clad pumping geometry in which, as mentioned above, effective absorption of the active laser center in the cladding is reduced significantly. As an example, in the case of Er^{3+}, it was suggested that Yb^{3+}, which has an intense and broad absorption band at 980 nm, can be a very good sensitizer. Experimental and theoretical research of the energy transfer between Yb^{3+} and Er^{3+} in different materials showed that direct excitation of Yb^{3+} produces a very efficient energy transfer to Er^{3+} in several laser glass hosts (see Fig. 2.7). In the case of the Yb^{3+}–Er^{3+} system, Yb^{3+} ions absorb pumping light in their broad absorption band at 980 nm, which follows an efficient energy transfer from the $^2F_{5/2}$ level of Yb^{3+} to the $^4I_{11/2}$ level of Er^{3+}. This is followed by fast nonradiative relaxation from the $^4I_{11/2}$ energy level to the metastable $^4I_{13/2}$ energy level. The $^4I_{13/2}$ energy level is an upper energy level of the 1,550 nm Er^{3+} fiber laser (see Fig. 2.7).

Concentration of Yb^{3+} is usually much higher than the concentration of Er^{3+} in such co-doped systems, which make pump absorption higher and give reasonable gain fiber lengths in case of clad-pumping geometry. In addition, 980-nm indium gallium arsenide (InGaAs) laser diodes are available with higher power models

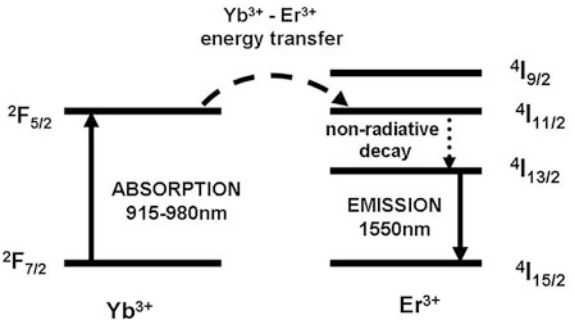

Fig. 2.7 Simplified excitation and energy transfer process in an Er^{3+}-doped glass sensitized with Yb^{3+}

and demonstrate much higher electrical to optical efficiency (>60 %) compared to ~25–30 % for 1,470–1,530-nm diode lasers used for direct Er^{3+} excitation. Unlike the case of Yb^{3+} sensitization, however, where there is a big quantum defect between pump and lasing photon energies, Er^{3+} fiber lasers with direct (i.e., resonant) excitation in the 1,450–1,550-nm spectral range may demonstrate high fiber-laser energy efficiency, high slope efficiency, and low quantum defects, which in turn reduce the heat generated by the laser medium. For high-power Er^{3+}-doped fiber laser systems, such resonant excitation plays a crucial role in solving the problem of thermal management of the laser system. However, when this approach is applied to clad pumping geometry, it requires achievement of high laser-active Er^{3+} concentration in laser glass with absent of luminescence quenching, which in turn is a challenging task. Because of the quasi-three-energy level (i.e., resonant nature) of the direct excitation of Er^{3+} when pumped directly into the 1,450–1,530-nm band, this approach requires higher pump power densities to reach transparency of the resonant Er^{3+} absorption in order to eliminate reabsorption of signal power and achieve positive net gain.

References

1. J.M. Pellegrino, W.M. Yen, M.J. Weber, Composition dependence of Nd^{3+} homogeneous line widths in glasses. J. Appl. Phys. **51**, 6332 (1980)
2. J.T. Fournier, R.H. Bartram, Inhomogeneous broadening of the optical spectra of Yb^{3+} in phosphate glass. J. Phys. Chem. Solids **31**, 2615–2624 (1970)
3. R.I. Laming, L. Reekie, P.R. Morkel, D.N. Payne, Multichannel cross talk and pump noise characterization of Er^{3+} doped fiber amplifiers pumped at 980 nm. Electron Lett. **25**, 455–456 (1989)
4. E. Desurvire, J.L. Zyskind, J.R. Simpson, Spectral gain hole-burning at 1.53 um in erbium-doped fiber amplifiers. IEEE Photon. Technol. Lett. **2**(4), 246–248 (1990)
5. J.L. Zyskind, E. Desurvive, J.W. Sulho, D. DiGiovanni, Determination of homogeneous line-width by spectral gain hole-burning in an erbium-doped fiber amplifier with a GeO2-SiO2 core. IEEE Photon. Technol. Lett. **2**(12), 869–871 (1990)
6. F. Roy, D. Bayart, C. Heerdt, A.L. Sauze, P. Baniel, Spectral hole burning measurement thulium-doped fiber amplifiers. Opt. Lett. **27**(1), 10–12 (2002)
7. B.R. Judd, Optical absorption intensities of rare-earth ions. Phys. Rev. **127**, 750–761 (1962)
8. G.S. Ofelt, Intensities of crystal spectra of rare-earth ions. J. Chem. Phys. **37**, 511–520 (1962)
9. C.W. Nielson, G.F. Koster, *Spectroscopic Coefficients for the p^n, d^n and f^n Configurations* (MIT Press, Cambridge, MA, 1963)
10. R. Reisfeld, in *Spectroscopy of Solid-State Laser-Type Materials*, ed. by B.D. Bartolo (Plenum Press, New York, 1987), pp. 343–396
11. R. Reisfeld, G. Katz, N. Spector, C.K. Jorgensen, C. Jacohoni, R. de Pape, J. Sol. St. Chem. **41**, 253 (1982)
12. F. Auzel, Risita della statz. Sper. Vetro **5**, 49 (1990)
13. M.J. Weber, T.E. Varitimos, B.H. Matsinger, Optical intensities of rare-earth ions in yttrium orthoaluminate. Phys. Rev. B **8**, 47 (1973)
14. W.J. Miniscalco, *Rare Earth Doped Fiber Lasers and Amplifiers* (Marcel Dekker, Inc., New York, 1993), p. 33

15. C. Gorrller-Walrand, K. Binnemans, *Handbook on the Physics and Chemistry of Rare Earths*, vol. 25 (Elsevier Science, 1998), p. 167
16. D.E. McCumber, Theory of phonon-terminated optical lasers. Phys. Rev. **134**(2A), A299–A306 (1964)
17. W.J. Miniscalco, R.S. Quimby, General procedure for the analysis of Er^{3+} cross sections. Opt. Lett. **16**(4), 258–260 (1991)
18. P.H. Sarkies, J.N. Sandoe, S. Parke, Variations of Nd^{3+} cross section for stimulated emission with glass composition. J. Phys. D: Appl. Phys. **4**(10), 1642–1649 (1971)
19. J.N. Sandoe, P.H. Sarkies, S. Parke, Variation of Er^{3+} cross section for stimulated emission with glass composition. J. Phys. D: Appl. Phys. **5**, 1788–1799 (1972)
20. J. Dong, M. Bass, C. Walters, Temperature-dependent stimulated-emission cross section and concentration quenching in Nd^{3+}-doped phosphate glasses. J. Opt. Soc. Am. B **21**, 454–457 (2004)
21. A. C. Erlandson, G. F. Albrecht, S. E. Stokowski, Model predicting the temperature dependence of the gain coefficient and the extractable stored energy density in Nd:phosphate glass lasers. J. Opt. Soc. Am. B **9**, 214–222 (1992).
22. P. Babu, H.J. Seo, K.H. Jang, R. Balakrishnaiah, C.K. Jayasankar, K.-S. Lim, V. Lavín, Optical spectroscopy, 1.5 μm emission, and upconversion properties of Er^{3+}-doped metaphosphate laser glasses. J. Opt. Soc. Am. B **24**, 2218–2228 (2007)
23. M. Jayasimhadri, L.R. Moorthy, K. Kojima, K. Yamamoto, N. Wada, Er-doped tellurofluorophosphate glasses for lasers and optical amplifiers. J. Phys. Condens. Matter. **17**, 7705–7717 (2005)
24. W.A. Pisarski, Spectroscopic analysis of praseodymium and erbium ions in heavy metal fluoride and oxide glasses. J. Mol. Struct. **744–747**, 473–479 (2005)
25. C. Laxmi kanth, B.V. Ragavaiah, B. Appa Rao, N. Veeraiah, Optical absorption, fluorescence and thermoluminescence properties of ZnF2-MO-TeO2 (MO = ZnO, CdO and PbO) glasses doped with Er ions. J. Lumin **109**, 193–205 (2004)
26. X. Qiao, X. Fan, M. Wang, X. Zhang, Up-conversion luminescence and near infrared luminescence of Er^{3+} in transparent oxyfluoride glass-ceramics. Opt. Mater. **27**, 597–603 (2004)
27. H. Lin, K. Liu, E.Y.B. Pun, T.C. Ma, X. Peng, Q.D. An, J.Y. Yu, S.B. Jiang, Infrared and visible fluorescence in Er-doped gallium tellurite glasses. Chem. Phys. Lett. **398**, 146–150 (2004)
28. D. Ning, Y. Iv-yun, P. Ming-ying, Z. Qing-ling, C. Dan-ping, T. Akai, K. Kadono, Preparation and spectroscopic properties of Er^{3+}-doped high silica glass by sintering nanoporous glass. Mater. Lett. **60**, 1987–1989 (2006)

http://www.springer.com/978-3-319-02337-3

Fundamentals of Fiber Lasers and Fiber Amplifiers

Ter-Mikirtychev, V.

2014, XXI, 253 p. 132 illus., Hardcover
ISBN: 978-3-319-02337-3